Origin of the Overpotential for Oxygen Reduction at a Fuel-Cell Cathode

J. K. Nørskov,* J. Rossmeisl, A. Logadottir, and L. Lindqvist

Center for Atomic-scale Materials Physics, Department of Physics, Technical University of Denmark, DK-2800 Lyngby, Denmark

J. R. Kitchin

Department of Chemical Engineering, University of Delaware, Newark, Delaware 19716

T. Bligaard

Science Institute, VR-II, University of Iceland, IS-107 Reykjavík, Iceland

H. Jónsson

Faculty of Science, VR-II, University of Iceland, IS-107 Reykjavík, Iceland

Received: June 18, 2004; In Final Form: September 2, 2004

We present a method for calculating the stability of reaction intermediates of electrochemical processes on the basis of electronic structure calculations. We used that method in combination with detailed density functional calculations to develop a detailed description of the free-energy landscape of the electrochemical oxygen reduction reaction over Pt(111) as a function of applied bias. This allowed us to identify the origin of the overpotential found for this reaction. Adsorbed oxygen and hydroxyl are found to be very stable intermediates at potentials close to equilibrium, and the calculated rate constant for the activated proton/electron transfer to adsorbed oxygen or hydroxyl can account quantitatively for the observed kinetics. On the basis of a database of calculated oxygen and hydroxyl adsorption energies, the trends in the oxygen reduction rate for a large number of different transition and noble metals can be accounted for. Alternative reaction mechanisms involving proton/electron transfer to adsorbed molecular oxygen were also considered, and this peroxide mechanism was found to dominate for the most noble metals. The model suggests ways to improve the electrocatalytic properties of fuel-cell cathodes.

Introduction

Low-temperature fuel cells are attracting considerable interest as a means of producing electricity by direct electrochemical conversion of hydrogen and oxygen into water.[1] There are, however, severe shortcomings of the present technology, which need to be overcome to make low-temperature fuel cells more economically attractive. One of the most important problems is related to the low rate of the cathode reaction where oxygen is reduced

$$\frac{1}{2}O_2 + 2(H^+ + e^-) \rightarrow H_2O \qquad (1)$$

Pt is the commonly used electrode material, but there is a considerable overpotential associated with this reaction over Pt. For some reason, the kinetics of the cathode reaction make it much slower than the anode reaction,

$$H_2 \rightarrow 2(H^+ + e^-) \qquad (2)$$

and there is presently no consensus why this is so.[1,2]

In the following, we use density functional theory (DFT) calculations to gain some insight into the cathode reactions. DFT calculations can provide information about the stability of surface intermediates in the reactions, which cannot be easily obtained by other means. We start by considering the simplest possible reaction mechanism over a Pt(111) surface. We introduce a method for calculating the free energy of all intermediates as a function of the electrode potential directly from density functional theory calculations of adsorption energies for the surface intermediates. On this basis, we establish an overview of the thermodynamics of the cathode reaction as a function of voltage, and we show that the overpotential of the reaction can be linked directly to the proton and electron transfer to adsorbed oxygen or hydroxide being strongly bonded to the surface at the electrode potential where the overall cathode reaction is at equilibrium. We introduce a database of density functional theory calculations of energies of the surface intermediates for a number of metals and show that, on this basis, we can establish trends in the thermodynamic limitations for all the metals in question. The model predicts a volcano-shaped relationship between the rate of the cathode reaction and the oxygen adsorption energy. The model explains why Pt is the best elemental cathode material and why alloying can be used to improve its performance.[3−7]

The Simplest Model

To introduce the basic concepts, we first study the simple dissociative mechanism

* Corresponding author. E-mail: norskov@fysik.dtu.dk.

10.1021/jp047349j CCC: $27.50
Published on Web 10/22/2004

$$\frac{1}{2}O_2 + * \rightarrow O* \quad (3)$$

$$O* + H^+ + e^- \rightarrow HO* \quad (4)$$

$$HO* + H^+ + e^- \rightarrow H_2O + * \quad (5)$$

Here, * denotes a site on the surface. Later, we will also discuss in detail the associative mechanism where O_2 does not dissociate before it is hydrogenated, and we will show that although this changes several important details of the reaction kinetics, it does not affect the main conclusions, in particular, regarding the overall variations in the reaction rate from one metal to the next.

The stability of the intermediates O* and HO* can be calculated on a Pt(111) surface. In Table 1, we show the calculated binding energies defined as the reaction energies of the reactions

$$H_2O + * \rightarrow HO* + {}^1/_2\,H_2 \quad (6)$$

$$H_2O + * \rightarrow O* + H_2 \quad (7)$$

where H_2O and H_2 are in the gas phase. The stability of both adsorbed OH and adsorbed O depends strongly on the oxygen coverage; therefore in Table 1, we include results for two different oxygen coverages to illustrate this effect.

We now introduce our procedure for calculating the free energy of the intermediates of the electrochemical reactions (eqs 3−5). It goes in six steps:

1. By setting the reference potential to be that of the standard hydrogen electrode, we can relate the chemical potential (the free energy per H) for the reaction ($H^+ + e^-$) to that of ${}^1/_2H_2$ (eq 2 is in equilibrium). This means that, at pH = 0 in the electrolyte and 1 bar of H_2 in the gas phase at 298 K, the reaction free energies of eqs 6 and 7 are equal to those of the reverse reactions eq 5 and eq 4 + 5 at an electrode potential of $U = 0$ relative to the standard hydrogen electrode.

2. To model the water environment of the electrochemical cell, we include the effect of a monolayer of water on the stability of adsorbed O and OH in the calculation. For the low coverage results, we have simply added water to fill the surface, and we have added bilayer of water on top of the adsorbed O and OH for the high coverage results as proposed by Ogasawara et al.[12] The interaction with water stabilizes OH groups on the surface relative to adsorbed oxygen due to hydrogen bonding. The effect of the water layer on adsorped oxygen is negligible. This procedure can be improved by including more water in the calculation.

3. We include the effect of a bias on all states involving an electron in the electrode, by shifting the energy of this state by $-eU$, where U is the electrode potential.

4. The adsorbed states also interact with the field set up outside the surface by the electrochemical double layer. The most rigorous treatment would involve a detailed model of the water and two electrodes and the electrolytes with a bias. This would entail a calculation for a nonequilibrium system with two Fermi levels, which is not currently possible. A simple estimate of the field effect can be obtained by calculating the coupling between the dipole moment of the adsorbed state and the average field just outside the surface. For O* and OH*, this gives a small effect because the dipole moments are small, 0.035 and 0.05 eÅ, respectively, on Pt(111).[13] At a bias of 1 V relative to the point of zero charge, the typical average field is ∼0.3 V/Å, assuming the width of the double layer to be ∼3 Å. The effect of the electrical field on the adsorption energy is thus approximately 0.05 eÅ × 0.3 V/Å = 0.015 eV. We neglect this in the following.

TABLE 1: Binding Energies (ΔE) and Free Energies (ΔG) for Different Intermediates[a]

	ΔE		$\Delta E_{w,water}$		$\Delta G_{w,water}$ (300 K)	
	$\theta_O = 0$	$\theta_O = {}^1/_2$	$\theta_O = 0$	$\theta_O = {}^1/_2$	$\theta_O = 0$	$\theta_O = {}^1/_2$
H_2O(gas, 0.035 bar)	0		0		0	
$*OH + {}^1/_2H_2$ (1 bar)	**0.78**	**1.52**	**0.45**	**1.41**	0.80	1.76
$*O + H_2$	**1.53**	**2.36**	**1.53**	**2.36**	1.58	2.41
${}^1/_2O_2 + H_2$					2.46	

[a] The energies in bold were obtained from DFT calculations. Two oxygen coverages are considered, 0 and ${}^1/_2$ of a monolayer. In the latter case, the oxygen adsorption energy is the differential heat of adsorption and OH is bonded to the surface in the presence of half a monolayer of oxygen. At zero O coverage, the lowest energy state of OH is one with a coverage of ${}^1/_3$ and this is the value given. We have also included the effect of the water surroundings ($\Delta E_{w,water}$) as described in the text. The free-energy difference for the full reaction, eq 1, is taken from experiment (see p 307 of ref 8). This makes sure that this key number is correct, and it avoids a DFT calculation for the O_2 molecule. The high-spin ground state of this molecule is notoriously poorly described in DFT calculations.[9,10] All other energies are derived from these numbers using the entropies and zero point energies from Appendix 1. We use gas-phase H_2O and H_2 as reference states because they are readily treated in the DFT calculations. The entropy for H_2O is calculated at 0.035 bar because this is the equilibrium pressure of H_2O at 300 K.[11] The free energy of this state is therefore equal to that of liquid water.

5. At a pH different from 0, we can correct the free energy of H^+ ions by the concentration dependence of the entropy: $G(\mathrm{pH}) = -kT\ln[H^+] = kT\ln 10 \times \mathrm{pH}$.

6. We calculate free energies of the intermediates at zero potential and pH = 0 as $\Delta G = \Delta E_{w,water} + \Delta ZPE - T\Delta S$, where ΔE is the reaction energy of eq 6 or 7, ΔZPE is the difference in zero point energies due to the reaction, and ΔS is the change in entropy. All of the parameters have been taken from DFT calculations[14] or standard tables for gas-phase molecules[11,15] and are shown in Appendix 1.

The electronic structure problem has been solved using density functional theory in a plane wave pseudopotential implementation,[16,17] employing the ultra-soft pseudopotentials of Vanderbilt[18] to represent the ionic cores. All calculations were performed with the RPBE exchange-correlation functional[19] on periodically repeated metal slabs. The Pt calculations were done on a (3 × 2) three-layer fcc(111) slab at the RPBE lattice constant of Pt (4.02 Å) separated by at least five equivalent layers of vacuum. The bottom two layers were fixed, and the top layer was allowed to relax. A 3 × 4 × 1 Monkhorst−Pack k-point sampling was used. The plane wave cutoff was 340 eV, and the density was treated on a grid corresponding to a plane wave cutoff at 500 eV. For the results presented in Table 2, the OH adsorption energies were calculated on (2 × 2) four-layer slabs with the top two layers relaxed. A 4 × 4 × 1 Monkhorst−Pack k-point sampling was used, with maximum symmetry applied to reduce the number of k points in the calculations. The dipole correction was used in all cases. The plane wave cutoff was 340 eV for OH, 350 eV for H, and 450 eV for the O adsorption calculations.

Using the procedure outlined above, we construct the free-energy diagram at several electrode potentials U, Figure 1. (The idea of making such free-energy diagrams is not new to electrochemistry; see, e.g., Figure 1, page 304 of ref 8.) We first concentrate on the case where the oxygen coverage is small. The electrode potential measured relative to the standard

TABLE 2: Calculated Reaction Heats for Reaction 6 (ΔE_{OH}) and Reaction 7 (ΔE_O) over the Most Close Packed Surface of a Number of Metals at a Quarter Monolayer Coverage[a]

metal	ΔE_{OH} (eV)	ΔE_O (eV)	$\Delta G_0(U_0)$ (eV)	$\Delta G_1(U_0)$ (eV)	$\Delta G_2(U_0)$ (eV)	E_a^{diss} (eV)
Ag	0.72	2.12	−0.33	−0.43	0.76	0.93
Au	1.49	2.75	0.30	−0.29	−0.01	2.06
Co	−0.08	−0.22	−2.67	1.11	1.56	−3.29
Cu	0.37	1.20	−1.25	0.14	1.11	−0.73
Fe	−0.88	−0.90	−3.35	0.99	2.36	−4.51
Ir	0.63	1.00	−1.45	0.60	0.85	−1.09
Mo	−0.61	−1.62	−4.07	1.98	2.09	−5.81
Ni	0.13	0.34	−2.11	0.76	1.35	−2.28
Pd	0.92	1.53	−0.92	0.36	0.56	−0.14
Pt	1.05	1.57	−0.88	0.45	0.43	−0.06
Rh	0.34	0.44	−2.01	0.87	1.14	−2.10
Ru	−0.01	−0.05	−2.50	1.01	1.49	−2.98
W	−0.80	−2.06	−4.51	2.23	2.28	−6.60

[a] The free-energy differences take solvation, entropic, and zero point energies into account by adjusting the reaction free energies to reproduce the low coverage results on Pt observed in Table 1 and by using the same adjustment for all of the other surfaces. $\Delta G_0(U_0) = \Delta E_O - 2eU_0 + 0.01$ eV $= \Delta E_O - 2.45$ eV. $\Delta G_1(U_0) = \Delta E_{OH} - \Delta E_O + eU_0 - 0.26$ eV $= \Delta E_{OH} - \Delta E_O + 0.97$ eV. $\Delta G_2(U_0) = -\Delta E_{OH} + eU_0 + 0.25$ eV $= -\Delta E_{OH} + 1.48$ eV. We have calculated the activation energy for O_2 dissociation (the transition state energy between the molecularly adsorbed and the atomically adsorbed states) using the atomically adsorbed state energy ΔE_O and the linear relationship that has been established between this energy and the dissociative chemisorption energy.[24] (The dissociative chemisorption energy is $\Delta E_{O_2} = 2(\Delta E_O - 0.29$ eV$) - 4eU_0$ eV $= 2\Delta E_O - 5.51$ eV, and because the activation energy depends on the dissociative chemisorption energy as $E_a \approx 0.9\ \Delta E_{O_2} + 2.07$ eV[24], we get $E_a \approx 1.8\ \Delta E_O - 2.89$ eV).

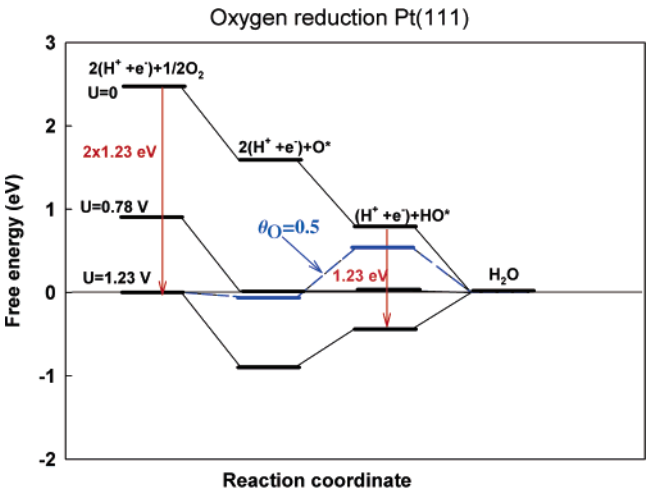

Figure 1. Free-energy diagram for oxygen reduction over Pt(111) based on the energies in Table 1. Results for low oxygen coverage are shown at zero cell potential ($U = 0$), at the equilibrium potential ($U = 1.23$ V), and at the highest potential ($U = 0.78$ V) where all reaction steps are exothermic. For $U = 1.23$ V, the free-energy diagram for the case of an oxygen coverage of $^1/_2$ is included.

hydrogen potential is equal to the potential of the fuel cell if we assume the anode reaction to be in equilibrium and neglect ohmic losses. The relationship $U = 0$ V corresponds to the reaction running by short circuiting the cell. This situation is roughly equivalent to the gas-phase hydrogen oxidation reaction, and all elementary steps are strongly exothermic. If, however, we shift the chemical potential of the electrons by the equilibrium potential of $U_0 = 1.23$ eV, corresponding to the situation where the fuel cell has the maximum potential allowed by thermodynamics, then both electron/proton-transfer steps (see the equations and point 5 above) become uphill. The barriers for the two steps are essentially the same. It is therefore likely that one of these is the rate-limiting step. There will be an activation free energy for the process, which is at least equal to the larger of the reaction free energies

$$\Delta G_1(U) = G_{HO^* + 1/2H_2}(U) - G_{O^*+H_2}(U) = \Delta G_1(0) + eU = \Delta G_1(U_0) - e\eta \quad (8a)$$

and

$$\Delta G_2(U) = G_{H_2O}(U) - G_{HO^*+1/2H_2}(U) = \Delta G_2(0) + eU = \Delta G_2(U_0) - e\eta \quad (8b)$$

where $\eta = U_0 - U$ is the overpotential. In other words, adsorbed oxygen and hydroxide on the Pt(111) surface are thermodynamic sinks for the oxygen reduction process, and the activation energy for the total process at the maximum cell voltage $U_0 = 1.23$ V is at least $\Delta G_1(U_0) = 0.45$ eV (Table 1 and Figure 1). This value is, indeed, close to the experimentally observed overpotential.[2]

Figure 1 also shows that the opposite process, the dissociation of water into OH or O, will be uphill at potentials up to 0.78 V. After that it is down hill, and water should dissociate. This is in excellent agreement with experiment.[29] The potential at which water dissociates spontaneously is also the point at which the proton/electron transfer to adsorbed O and OH becomes activated and the oxygen reduction process starts becoming slow. The onset of water dissociation and the overpotential for the oxygen reduction process are therefore, in this picture, two sides of the same phenomenon.

Although we cannot deduce the detailed kinetics from the thermodynamic data of Table 1 and Figure 1, we can develop a simple model of the electrode kinetics in the following way. We will assume, for simplicity, that the activation barrier for the rate-limiting proton-transfer step is equal to the larger of the free-energy differences, eqs. 8a and 8b. Detailed calculations for the transfer of a solvated proton to adsorbed OH show this to be a very good approximation for a situation where the proton transfer is down hill in energy.[20] At other potentials, there may be an extra barrier, which will have to be included. In the case where the is no extra barrier, the rate constant for the reaction can be written as

$$k(U) = k_0 e^{-\Delta G(U)/kT} \quad (9)$$

where $\Delta G(U)$ is the larger of the two free-energy steps in eqs 8a and 8b. The prefactor, k_0, includes all of the details of the proton transfer to the surface and recombination with the electron. In units of current density, the rate constant is

$$i_k(U) = 2e\frac{N_{sites}}{A}k(U) \quad (10)$$

where N_{sites}/A is the number of sites per surface area. Equations 9 and 10 can be expressed as

$$i_k(U) = \tilde{i}_k e^{-\Delta G(U)/kT} \quad (11)$$

This equation represents an upper bound to the rate; however, if there are additional barriers to the proton transfer or if the coverage is far from ideal, this would slow the reaction.

We can take the prefactor k_0 from measured values of the proton-transfer rate to metal surfaces under conditions where there is no driving force (the exchange current). This gives a value of $k_0 \approx 200$ s^{-1} site^{-1}; [21] hence, $\tilde{i}_k = 96$ mA cm^{-2}. The result of the simple model, with no parameters fitted to the

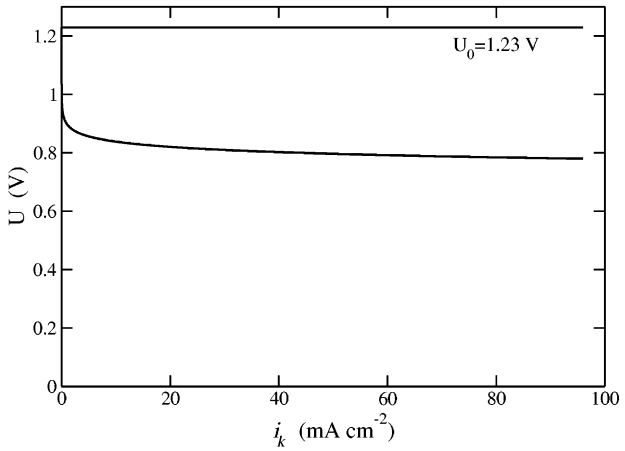

Figure 2. Calculated potential vs the rate constant in units of current density from the model, eqs 8−11.

oxygen reduction data, is shown in Figure 2. When the simplicity of the model and the approximate nature of the DFT calculations are taken into account, the similarity to experimental data for the potential as a function of rate constant in units of current density for a fuel cell is convincing.[2]

We note that we can rewrite eqs 9−11 in the following way

$$i_k(U) = i_k^0 e^{e\eta/kT} \tag{12}$$

where the exchange current rate constant is

$$i_k^0 = \tilde{i}_k e^{-\Delta G(U_0)/kT} \tag{13}$$

This leads to the usual Butler−Volmer type relation

$$U = U_0 - b \log_{10}\left(\frac{i_k}{i_k^0}\right) \tag{14}$$

where the Tafel slope is $b = kT \ln 10/e = 60$ mV at 300 K (71 mV at 357 K). This value is consistent with experiment for both Pt surface and the catalyst.[1,2,22,23]

A more detailed model would include the bias dependence of the oxygen coverage and, hence, the coverage-dependent oxygen adsorption energy. Without going into a detailed evaluation of the oxygen coverage, we illustrate the effect of a higher coverage in Figure 1, where we have included data for oxygen coverage of 0.5 at the equilibrium cell potential. Clearly, the energies are shifted up, and it is now clear that the first electron and proton transfer has the higher barrier, but the value of the barrier is surprisingly independent of the coverage.

When the potential has been decreased by approximately the overpotential, the otherwise rate-limiting proton transfer becomes nonactivated, and the associated rate constant loses its potential dependence and is given entirely by its prefactor. The Tafel slope must therefore start decreasing at low values of U because the (in this regime) potential-independent rate constant leads to a saturation of the current density and, hence, to larger values of b. More detailed modeling, including coverages determined self-consistently as a function of the potential, will be presented elsewhere.

Other Metals

We can use the simple picture developed above to investigate the oxygen reduction reaction on other metals than Pt. To this end, we have made DFT calculations to get the bond energies of O* and HO* for a number of interesting metals, Table 2.

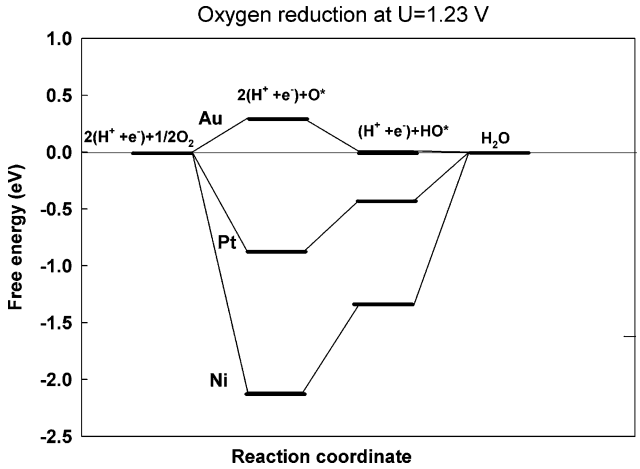

Figure 3. Free-energy diagram for oxygen reduction at the equilibrium potential $U_0 = 1.23$ V over Pt, Au, and Ni.

From this, we can evaluate $\Delta G_1(U_0)$ and $\Delta G_2(U_0)$ for the metals involved. It is the larger of the two that determines the overpotential for the proton-transfer reactions. It can be seen from the table that there is a substantial variation in the overpotential. If we exclude Cu, Ag, and Au, then Pt and Pd stand out as the metals with the smallest overpotentials, followed by Ir and Rh. This is in good agreement with experimental evidence.[1,2]

Figure 3 shows why metals that have either stronger or weaker bonding of oxygen than Pt are poorer oxygen-reduction catalysts. At the equilibrium cell potential, Ni binds O and OH so strongly on the surface that the proton-transfer steps become strongly activated, and thus very slow. For Au, however, the proton transfer is exothermic and should be fast, but oxygen on the surface is considerably less stable than it is in the gas phase; therefore, no transfer of protons and electrons to oxygen can occur. In fact, the problem for Au is even worse. The weak bonding of atomic oxygen is an indication that the barrier for oxygen dissociation is large. It has been shown that there is a linear dependence between the oxygen binding energy and the barrier for oxygen dissociation.[24] In Table 2, we include an estimate of the activation barrier for oxygen dissociation. For Au and Ag, this is the largest energy barrier in the problem, for the simple dissociative reaction mechanism considered so far.

To analyze this in further detail, we constructed an activity measure based on a microkinetic model. The rate constant for the forward direction of the elementary reaction step i is

$$k_i = \nu_i e^{-E_a^i/kT} \tag{15}$$

if step i is activated. Assuming that the rate-limiting reaction step has full coverage of the reactant surface sites (free sites for O_2 dissociation, O sites for oxygen hydrogenation, and OH sites for hydrogenation of hydroxyl groups) enables us to define a measure of maximal activity, A

$$A = kT \min_i\left(\log\left(\frac{k_i}{k_0}\right)\right) \tag{16}$$

where k_0 normalizes the activity of nonactivated electron/proton transfer to zero. This is an application of the concept of Sabatier Analysis,[25] which is a useful tool for studying trends in heterogeneous catalysis.

The prefactor for O_2 dissociation is somewhat larger than the prefactor for the hydrogenation steps. This leads to an increased activity for this elementary step. Assuming that all

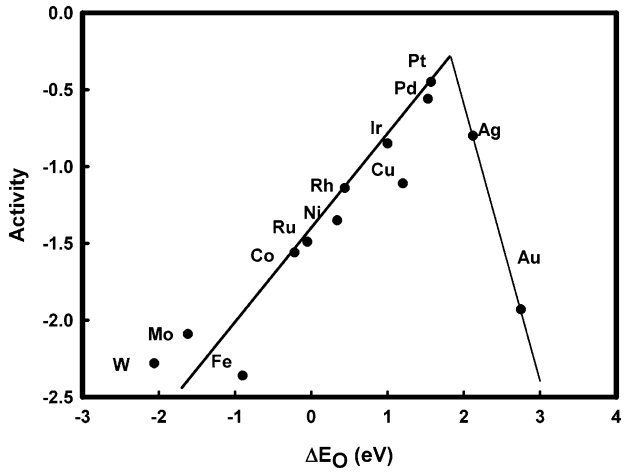

Figure 4. Trends in oxygen reduction activity (defined in the text) plotted as a function of the oxygen binding energy.

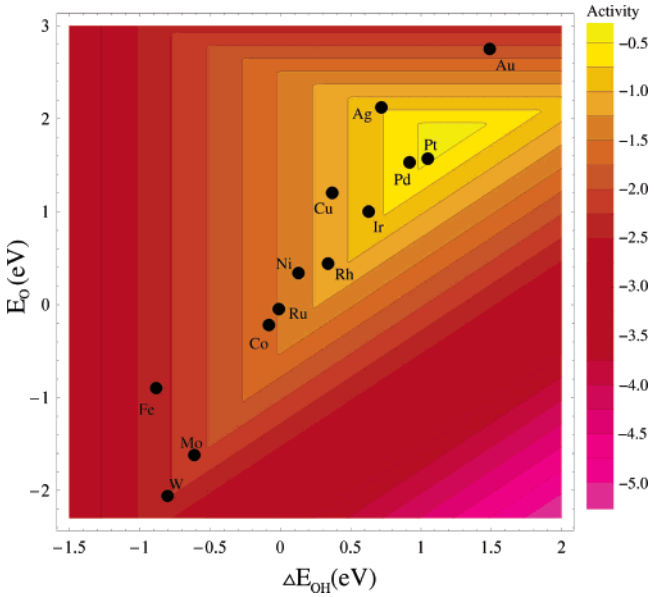

Figure 5. Trends in oxygen reduction activity plotted as a function of both the O and the OH binding energy.

entropy is lost in the transition state for dissociation, the prefactor for dissociative chemisorption as determined from rate theory is $\nu_{diss} = (kT/h)(1/q_{gas})$. Taking only translational and rotational contributions to the partition function q_{gas} into account, we obtain

$$q_{gas} = \frac{kT}{2\epsilon_{rot}} \frac{kT}{P_{O_2}} \left(\frac{2\pi m_{O_2} kT}{h^2}\right)^{3/2} \tag{17}$$

where $\epsilon_{rot} = 0.179$ meV is the rotational constant for O_2. The activity for O_2 dissociation is thus increased compared to hydrogenation at similar barrier by $kT \log(\nu_{diss}/k_0) \approx 0.13$ eV at 1 bar and 300 K.

The activities constructed from Table 2 are plotted in Figure 4 as a function of the O binding energy and in Figure 5 as a function of both the O and the OH binding energies. A nice volcano appears. In good agreement with experiment,[1,2] it shows that Pt and Pd are the best catalysts for oxygen reduction.

The volcano plot in Figure 4 shows that there is some room for improvement. Metals with a somewhat lower oxygen binding energy than Pt should have a higher rate of oxygen reduction. DFT calculations have shown that Pt alloys with, for example, Ni, Co, Fe, and Cr (where Pt will segregate to the surface[26]) have smaller oxygen binding energies than pure Pt.[27,28] (The OH binding energies are not reduced to the same extent on these surfaces. On a Pt monolayer over a monolayer of Ni, Co, or Fe on a Pt substrate, DFT calculations give $(\Delta E_{OH}, \Delta E_O) = (1.15$ eV, 1.89 eV), (1.06 eV, 2.00 eV), and (0.85 eV, 2.06 eV), respectively. This is to be compared to the adsorption on a pure Pt surface: $(\Delta E_{OH}, \Delta E_O) = (1.05$ eV, 1.57 eV).) Yu et al.[27] have shown that a Pt skin on top of $Pt_3Co(111)$ has an oxygen binding energy that is 0.38 eV less than that on pure Pt(111). It can be seen from Figure 4 that this should give a higher reactivity. The calculations of Kitchin et al.[28] show the same trends when including a number of 3d metals below the surface of Pt(111), but here, the absolute magnitudes cannot be used directly to compare to Figure 4 because these are idealized structures with no real alloy in the bulk and no alloying in the 3d underlayer. This beautifully explains the experimental observations that skins of Pt on these alloys have a higher rate than pure Pt.[29−33] Defects and steps on Pt would not be expected to improve the activity of the cathode because oxygen on these sites is bound stronger than on the flat surface, for example, on Pt(110), oxygen is bound 0.5 eV stronger.

It should be stressed in this context that it is not just the oxygen binding energy that determines the activity of a surface for oxygen reduction; the OH bonding energy is also important. It can be observed in Figure 5 that the two are roughly linearly correlated for the elemental surfaces. There are, however, ample possibilities for finding new systems where bonding of O and OH do not follow the same correlation and could lead to completely new catalysts for this important reaction.

The Associative Mechanism

The study of trends above is quite simple, and in the present section, we will refine it in two ways by including the possibility that O_2 does not dissociate before it is hydrogenated and the bias dependence of the volcano; explicitly, the volcano in Figure 4 is for the equilibrium bias, $U = 1.23$ V. Although these effects are important for the details, we will show that they do not affect the overall trends.

At potentials and oxygen coverages where O_2 dissociation is activated, it is possible that another reaction mechanism may take over, one that does not involve O_2 dissociation. In the following, we explore this possibility. Several authors have suggested that oxygen reduction on Pt surfaces takes place via peroxy intermediates,[29,33−37] for example, in a reaction given by the elementary steps

$$O_2 + * \rightarrow O_2* \tag{18}$$

$$O_2* + (H^+ + e^-) \rightarrow HO_2* \tag{19}$$

$$HO_2* + (H^+ + e^-) \rightarrow H_2O + O* \tag{20}$$

$$O* + (H^+ + e^-) \rightarrow HO* \tag{21}$$

$$HO* + (H^+ + e^-) \rightarrow H_2O + * \tag{22}$$

Steps 21 and 22 are the same as steps 4 and 5 for the dissociative mechanism above. The new steps, 18−20, involve adsorption of molecular O_2 and direct proton/electron transfer to it and to OOH. We refer to this as the associative mechanism. An alternative to forming water in step 20 is to form hydrogen peroxide. The associative mechanism can therefore also be termed a peroxo mechanism.

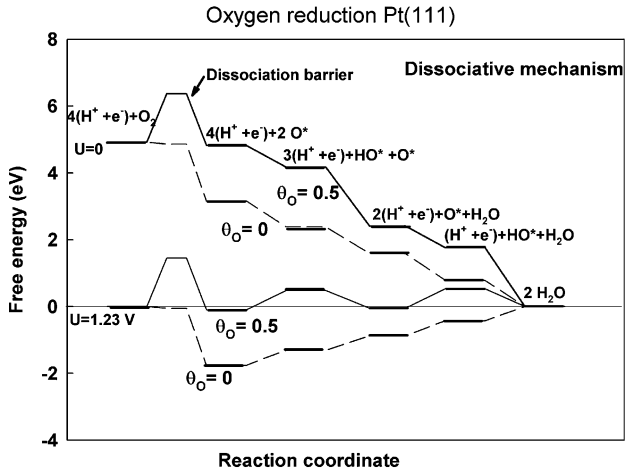

Figure 6. Free-energy diagram for oxygen reduction at two different potentials and at two different oxygen coverages, including the barrier for O_2 dissociation.

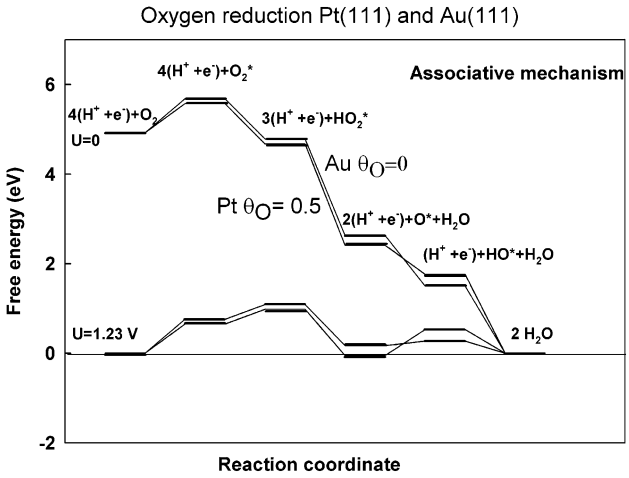

Figure 7. Free-energy diagram for oxygen reduction by the peroxide mechanism at two different potentials over Au(111) at a low oxygen coverage and over Pt(111) at an oxygen coverage of $^1/_2$.

In Figure 7, we show the calculated potential-energy diagram for the associative mechanism. The procedure is exactly the same as that for the dissociative reaction scheme, Figure 6. It can be seen that Au(111) at low oxygen coverage and Pt(111) at high oxygen coverage, the associative mechanism has lower free-energy barriers than the dissociation mechanism. For Pt at low oxygen coverages, the O_2 dissociation is not activated and the dissociative mechanism has the lowest barriers and dominates, Figure 6.

We can include the associative mechanism in the measure of maximal activity, *A*, eq 16. This is done in Figure 8. In Figure 8, we have also explicitly included the bias dependence of the activities.

There are three regimes visible in the kinetics: (I) the left leg, where the proton transfer to adsorbed O or OH is rate limiting, (II) a middle region where the dissociation is rate limiting, and (III) the right leg where the proton and electron transfer to adsorbed O_2 is rate limiting. Note that, in this region, the dissociative mechanism may be operative but at a much lover rate (compare the dashed and full lines to the right in the diagram). Region II is not present at all biases. At potentials of about 0.8 V and below, the associative mechanism dominates over the dissociation path, which means that at realistic overpotentials the two mechanisms should run in parallel.

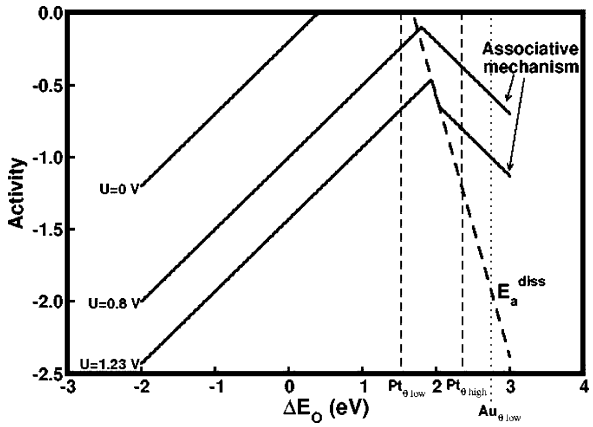

Figure 8. Trends in oxygen reduction activity plotted as a function of the oxygen binding energy at $U = 0$, 0.8 V, and 1.23 V. The activity corresponding to the associative mechanism has been included. Because the associative mechanism will be competing with the direct dissociation mechanism, the higher of these two activities will dominate the overall rate of the right leg of the volcano. The activity has been calculated using the linear relations defined in the captions of Table 2, and that $\Delta E_{OH} \approx 90.5\Delta E_{O_2} + 0.05$ eV and $\Delta E_{OOH} \approx 0.5\Delta E_{O_2} + 3.18$ eV. The activation energy for the associative reaction is ΔG_{assoc} (U) $\approx \Delta E_{OOH} + eU - 4.92$ eV $+ 0.18$ eV $= 0.5\Delta E_{O_2} - 1.56$ eV $+ eU$. At potentials below $U = 0.8$ V, the associative mechanism will dominate over the dissociation mechanism. The binding energies of oxygen on Pt at low and high oxygen coverage as well as Au at low oxygen coverage are depicted.

We note from Figure 8 that even when we include the possibility of the associative mechanism and explicitly include the bias dependence the maximum of the volcano hardly changes and that the trends discussed above for the volcanoes in Figures 4 and 5 remain valid.

Concluding Remarks

In the present paper, we have introduced a method to use density functional theory calculations to estimate the thermochemistry for electrochemical reactions. This part is completely general and should be applicable to any electrochemical reaction.

We then used the method to gain further insight into the electrochemical reduction of dioxygen. We have shown that for Pt(111) as electrode adsorbed oxygen tends to be so stable at high potentials that the proton and electron transfer becomes impossible. By lowering the potential, the stability of oxygen decreases and the reaction may proceed. This is suggested to be the origin of the overpotential for Pt.

We also used the calculations to compare dissociative and associative reaction paths and to conclude that both may contribute depending on the metal and the potential.

Finally, we have used the concept of a Sabatier Analysis[38] to introduce a measure of maximal catalytic activity and used that to construct volcano curves of the activity as a function of oxygen and hydroxyl adsorption energies. The resulting volcanoes describe known trends and rationalize observed effects of alloying.

Acknowledgment. We thank Radoslav R. Adzic for helpful discussions. The DFT calculations have been performed with support from the Danish Center for Scientific Computing through grant no. HDW-1101-05. We acknowledge financial support for A. Logadottir and T. Bligaard from the European Union through contract nos. ENK5-CT-2001-00572 and HPRN-CT-2002-00170, respectively.

TABLE 3: Zero Point Energy Corrections and Entropic Contributions to the Free Energies

	TS	*T*ΔS	ZPE	ΔZPE	ΔZPE − *T*ΔS
H_2O	.67	0	.56	0	0
$*OH + {}^1/_2H_2$	.20	−0.47	.44	−0.12	.35
$*O + H_2$	.41	−0.27	.34	−0.22	.05
$^1/_2O_2 + H_2$	.73	.05	.32	−0.24	−0.29
H_2	.41		.27		
$^1/_2O_2$	.32		.05		
O*	0		.07		
OH*	0		.30		
H*	0		.17		

Appendix 1

Entropies and zero point energies (ZPEs) are used in the construction of the reaction free energies throughout the paper (Table 3). The gas-phase values are from ref 15, and the values for the adsorbed species are taken from DFT calculations for O and OH adsorbed on Cu(111) by Mavrikakis et al.[14] We used gas-phase H_2O at 0.035 bar as the reference state because at this pressure, gas-phase H_2O is in equilibrium with liquid water at 300 K.[11]

References and Notes

(1) Markovic, N. M.; Ross, P. N. *CATTECH* **2000**, *4*, 110.
(2) Hoogers, G.; Thompsett, D. *CATTECH* **1999**, *3*, 106.
(3) Toda, T.; Igarashi, H.; Uchida, H.; Watanabe, M. *J. Electrochem. Soc.* **1999**, *146*, 3750.
(4) Sasaki, K.; Mo, Y.; Wang, J. X.; Balasubramanian, M.; Uribe, F.; McBreen, J.; Adzic, R. R. *Electrochim. Acta* **2003**, *48*, 3841.
(5) Stamenkovic, V.; Schmidt, T. J.; Ross, P. N.; Marković, N. M. *J. Electroanal. Chem.* **2003**, *554*−*555*, 191.
(6) Paulus, U. A.; Wokaun, A.; Scherer, G. G.; Schmidt, T. J.; Stamenkovic, V.; Markovic, N. M.; Ross, P. N. *Electrochim. Acta* **2002**, *47*, 3787.
(7) Antolini, E.; Passos, R. R.; Ticianelli, E. A. *Electrochim. Acta* **2002**, *48*, 263.
(8) Tarasevich, M. R.; Sadkowski, A.; Yeager, E. In Comprehensive Treatise of Electrochemistry, Conway, B., Bockris, J. O′. M., Yeager, E., Khan, S. U. M., White, R. E., Eds.; Plenum Press: New York, 1983; Vol. 7, Chapter 6..
(9) Jones, R. O.; Gunnarsson, O. *Rev. Mod. Phys.* **1989**, *61*, 689.
(10) Kurth, S.; Perdew, J. P.; Blaha, P. *Int. J. Quantum Chem.* **1999**, *75*, 889.
(11) *CRC Handbook of Chemistry and Physics*, 49th ed.; Weast, R. C. Ed.; The Chemical Rubber Company: Cleveland, OH, 1968−1969; p D109.
(12) Ogasawara, H.; Brena, B.; Nordlund, D.; Nyberg, M.; Pelmenschikov, A.; Pettersson, L. G. M.; Nilsson, A. *Phys. Rev. Lett.* **2002**, *89*, 276102.
(13) Liu, P.; Logadottir, A.; Nørskov, J. K. *Electrochim. Acta* **2003**, *48*, 3731.
(14) Kandoi, S.; Gokhale, A. A.; Grabow, L. C.; Dumesic, J. A.; Mavrikakis, M. *Catal. Lett.* **2004**, 93, 93.
(15) Atkins, P. W. *Physical Chemistry*, 6th ed., Oxford University Press: Oxford, U.K., 1998; pp 485, 925−927, 942.
(16) Payne, M. C.; Teter, M. P.; Allan, D. C.; Arias, T. A.; Joannopoulos, J. D. *Rev. Mod. Phys.* **1992**, *64*, 1045.
(17) Kresse G.; Furtmüller, J. *Comp. Mater. Sci* **1996**, *6*, 15.
(18) Vanderbilt, D. *Phys. Rev. B* **1990**, *41*, 7892.
(19) Hammer, B.; Hansen, L. B.; Nørskov, J. K. *Phys. Rev. B* **1999**, *46*, 7413.
(20) Desai, S. K.; Neurock, M. *Phys. Rev. B* **2003**, *68*, 75420.
(21) Nørskov, J. K.; Bligaard, T.; Logadottir, A.; Kitchin, J. R.; Chen, J. G.; Pandelov, S.; Stimming, U., submitted for publication.
(22) Markovic, N.; Gasteiger, H.; Ross, P. N. *J. Electochem. Soc.* **1997**, *144*, 1591.
(23) Paulus, U. A.; Schmidt, T. J.; Gasteiger, H. A.; Behm, R. J. *J. Electroanal. Chem.* **2001**, *495*, 134.
(24) Nørskov, J. K.; Bligaard, T.; Logadottir, A.; Bahn, S. R.; Hansen, L. B.; Bollinger, M. V.; Bengaard, H. S.; Hammer, B.; Sljivancanin, Z.; Mavrikakis, M.; Xu, Y.; Dahl, S.; Jacobsen, C. J. H. *J. Catal.* **2002**, *209*, 275.
(25) Bligaard, T.; Nørskov, J. K.; Dahl, S.; Matthiesen, J.; Christensen, C. H.; Sehested, J. *J. Catal.* **2004**, *224*, 206.
(26) Ruban, A. V.; Skriver. H. L.; Nørskov, J. K. *Phys. Rev. B* **1999**, *59*, 15900.
(27) Xu, Y.; Ruban, A. V.; Mavrikakis, M. *J. Am. Chem. Soc.* **2004**, *126*, 4717.
(28) Kitchin, J. R.; Nørskov, J. K.; Barteau, M. A.; Chen, J. G. *J. Chem. Phys.* **2004**, *120*, 10240.
(29) Markovic, N. M.; Ross, P. N. *Surf. Sci. Rep.* **2002**, *45*, 117.
(30) Toda, T.; Igarashi, H.; Uchida, H.; Watanabe, M. *J. Electrochem. Soc.* **1999**, *146*, 3750.
(31) Stamenkovic, V.; Schmidt, T. J.; Ross, P. N.; Marković, N. M. *J. Phys. Chem. B* **2002**, *106*, 11970.
(32) Mukerjee, S.; Srinivasan, S.; Soriaga, M.; McBreen, J. *J. Electrochem. Soc.* **1995**, *142*, 1409.
(33) Grgur, B. N.; Markovic, N. M.; Ross, P. N. *J. Can. Chem.* **1997**, ***75***, 1465.
(34) Chatenet, M.; Cenies-Butel, L.; Aurousseau, M.; Durand, R.; Andolfatto, F. *J. Appl. Electrochem.* **2002**, *32*, 1131.
(35) Blizanac, B. B.; Lucas, C. A.; Gallagher, M. E.; Arenz, M.; Ross, P. N.; Markovic, N. M. *J. Phys. Chem. B* **2004**, *108*, 625.
(36) Adzic R. R.; Wang, J. X. *Solid State Ionics* **2002**, *150*, 105.
(37) Strabac, S.; Anastasijevic, N. A.; Adzic, R. R. *Electrochim. Acta* **1994**, *39*, 983.
(38) Bligaard, T.; Nørskov, J. K.; Dahl, S.; Matthiesen, J.; Christensen, C. H.; Sehested, J. *J. Catal.* **2004**, *224*, 206.